Tailored emission properties of ZnTe/ZnTe:O/ZnO core-shell nanowires coupled with an Al plasmonic bowtie antenna array

Kui-Ying Nie[1,3†], Xuecou Tu[1,†], Jing Li[1], Xuanhu Chen[1], Fang-Fang Ren[1,2,5*], Guo-Gang Zhang [4*], Lin Kang[1], Shulin Gu[1,6], Rong Zhang[1,5,6], Peiheng Wu[1], Youdou Zheng[1], Hark Hoe Tan[2], Chennupati Jagadish[2], Jiandong Ye [1,2,6*]

[1]*School of Electronic Science and Engineering, Nanjing University, Nanjing 210093, China*

[2]*Department of Electronic Materials Engineering, Research School of Physics and Engineering, The Australian National University, Canberra ACT 2601, Australia*

[3] *School of Physics and Engineering, Xingyi Normal University for Nationalities, Xingyi 562400, China*

[4] *Grünberg Research Centre, Nanjing University of Posts and Telecommunications, Nanjing 210003, China*

[5] *Collaborative Innovation Center of Advanced Microstructures, Nanjing University, Nanjing 210093, China*

[6] *Collaborative Innovation Center of Solid-State Lighting and Energy-Saving Electronics, Nanjing University, Nanjing 210093, China*

† Authors contribute equally to this work.

*Correspondence and requests for materials should be addressed to F.-F.R. (ffren@nju.edu.cn), G. G. Z. (ggzhang@njupt.edu.cn) and J. D. Y. (yejd@nju.edu.cn).

Abstract: The ability to manipulate light-matter interaction in semiconducting nanostructures is fascinating for implementing novel functionalities in advanced optoelectronic devices. Here, we report the tailoring of radiative emissions in a ZnTe/ZnTe:O/ZnO core-shell single nanowire coupled with one-dimensional aluminum bowtie antenna array. The plasmonic antenna enables remarkable changes in the excitation and emission processes, leading to an obvious enhancement of near band edge emission (2.2 eV) and sub-gap excitonic emission (1.7 eV) bound to intermediate band states in ZnTe/ZnTe:O/ZnO core-shell nanowire as well as surface-enhanced Raman scattering at room temperature. The increase of emission decay rate in the nanowire/antenna system, probed by time-resolved photoluminescence spectroscopy, yields an observable enhancement of quantum efficiency induced by local surface plasmon resonance. Electromagnetic simulations agree well with the experimental observations, revealing a combined effect of enhanced electric near-field intensity and the improvement of quantum efficiency in ZnTe/ZnTe:O/ZnO nanowire/antenna system. The capability of tailoring light-matter interaction in low-efficient emitters may open up a new strategy for designing novel optoelectronic and sensing devices with precisely controlled response.

Keywords: plasmonic antennas, nanowires, exciton-plasmon coupling

The understanding and manipulation of light-matter interaction in polar semiconductors is of great importance for various promising applications in linear and nonlinear optoelectronic devices.[1-3] Localized surface plasmon resonance (LSPR) occurring in metallic nanostructures produces collective charge oscillations upon interaction with light and introduces strong resonant fields in their vicinity. It offers a powerful platform for near-field enhancement and confinement at the subwavelength scale.[4,5] To date, great efforts have been devoted to realize active manipulation of light emissions and even lasing by utilizing plasmon-induced hot carrier transfer under the excitation of LSPR.[6-9] In particular, plasmon-coupled exciton emissions with amplified intensities has been demonstrated in II-VI polar semiconducting nanostructures (such as ZnO, CdS and CdTe) due to the strong coupling of excitons to LO phonons and/or external plasmonic polariton via long-range Frohlich interaction, which leads to a much faster carrier radiative rate than the nonpolar semiconductors. [10]

Among the II-VI semiconductor family, ZnTe material has unique advantages of being intrinsically p-type with a direct bandgap of 2.26 eV, which is regarded as one of the most promising material for optoelectronic and energy-harvesting devices in the green spectral region.[10] In particular, ZnTe:O material by oxygen isoelectronic alloying exhibits a broad sub-bandgap absorption and a strong excitonic emission around 1.8 eV.[11] It has many promising applications such as green light emitting diodes, phosphors, intermediate band solar cells, and bright scintillator for high resolution X-ray imaging.[12-15] Recently, to harvest a wide portion of sunlight, optical engineering to tune the bandgap by using nanostructures and integrating metallic plasmonic structures has been demonstrated with enhanced sub-bandgap absorption and photoanodic response.[13,16] Despite of the efforts in energy-harvesting applications, little dedication has been made in the manipulation of excitonic emission in ZnTe material. Strong exciton-phonon coupling in ZnTe nanobelts was demonstrated to significantly enhance the exciton radiative decay rates.[10] However, as compared to other II-VI high efficient emitting materials, the quantum yield of ZnTe nanostructures is lower with a recorded value up to 60%.[17-19] The excitonic emission bound to the intermediate band states is also still below the demand

for the practical application due to its low density of states and low quantum efficiency.[17] To solve this problem, plasmonic coupling with metallic nanostructures is an alternative way for transferring energy and manipulating optical properties of low-efficient emitters.[20] "Bowtie" antennas, a sort of dimer nanoantennas with strong geometric resonances, have been proven to achieve high quantum efficiency while keeping nonradiative absorption weaker and large local field enhancement in the narrow gap between two coupled metallic nanostructures.[21-22] These lithographically fabricated plasmonic resonators are controllable and amenable to integration. In this manner, light-matter interaction can be tuned to significantly enhance the quantum yield of low-efficiency emitters and enable a whole new suite of optoelectronic applications with precisely tailored responses.[5,23]

Here, we demonstrate the manipulation of radiative emission from a ZnTe/ZnTe:O/ZnO core-shell single nanowire integrated with an aluminum (Al) plasmonic bowtie antenna array. Through coupling with the local surface plasmons (LSPs), both excitation and emission processes are modified in ZnTe/ZnTe:O/ZnO nanowire/antenna system with observations of surface-enhanced photoluminescence and surface-enhanced Raman scattering. With careful design and precisely controlled dimension of the hybrid nanowire/antenna structure, both near-band-edge (NBE) emission and excitonic emissions bound to oxygen-related intermediate band states are simultaneously amplified as result of the energy matching between radiative emissions and dielectric/plasmonic resonances. Electromagnetic simulations are consistent with the experimental observations, confirming that strong LSPR modes formed in the bowtie antenna enhances the electric near-field intensity and strengthens exciton-plasmon coupling within nanowires.

Fig.1 (a) shows that ZnTe nanowires with large length/diameter ratios were grown along (111) direction by chemical vapor transport technique on GaSb substrate, which has been described in details in the Methods section. ZnTe nanowires were mechanically transferred onto a SiO_2/Si substrate and the single one with an optimal diameter of 180 nm was selected for integration with an Al bowtie antenna (Fig.1 (b)). The bright and discrete spots in the selective-area-electron-diffraction pattern

shown in the inset of Fig.1 (b) indicates the ZnTe nanowire exhibits relatively high crystalline quality but containing stacking faults. Particular care was taken to control the oxidization of the transferred ZnTe nanowire, forming a p-i-n ZnTe/ZnTe:O/ZnO heterojunction perpendicular to the growth direction. The band structure schematic of p-ZnTe/i-ZnTe:O/n-ZnO is shown in Fig.1 (c). Owing to the diffusion process, oxygen composition in the ZnTe:O section is graded and thus the corresponding band structure has a potential gradient from n-ZnO shell (10 nm in thickness) to the un-reacted p-ZnTe core. Subsequently, one dimensional Al bowtie antenna arrays consisting of multiple pairs of two opposing tip-to-tip triangles (width w, height h) were designed and fabricated surrounding the single core-shell nanowire (ZnTe:O diameter d_1, ZnTe:O/ZnO diameter d_2=d_1+20 nm, length L). The bowtie antenna array is placed with a 90º-apex angle with a gap of about 200-nm as defined in Fig. 1(e). It was reported that the patterning of bowties into a periodic array leads to narrower LSPR linewidths with an enhanced light focusing capability.[24-26] Fig. 1 (d) shows the nanowire-antennas hybrid structures was achieved with ZnTe/ZnTe:O/ZnO core-shell nanowire located within the gap of Al bowtie antenna arrays.

Polarization and power dependent photoluminescence (PL) characterizations are used to investigate the manipulation of optical properties of ZnTe/ZnTe:O/ZnO core-shell nanowire by antenna coupling. All PL measurements were carried out at room temperature on a long ZnTe/ZnTe:O/ZnO core-shell nanowire with a uniform diameter of 180 nm, half of which was sandwiched by the Al bowtie antenna array whilst another half located outside the antenna. The polarized photoluminescence characteristics are shown in Supplementary Information Fig. S1. Because of the particular geometry of the nanowire, the near band emission around 550 nm of the bare nanowire exhibits a high polarization anisotropy with a large polarization ratio over 0.8. In high aspect ratio NWs, the longitudinal polarization is always more efficient than the transverse polarization in establishing the internal electric field. Furthermore, for smaller diameter nanowires anisotropy in the absorption behavior becomes more prominent. [27] The bowtie antenna strongly concentrate incident light with

transverse polarization and significantly alter their polarization sensitive optical behavior. [23] As a result, the emission polarization anisotropy in the nanowire/antenna structure is suppressed, as shown in Fig. S1 (c). It demonstrates that the designed metallic nanostructures offer us the possibility to tailor the electromagnetic coupling regime between nanowires and nanoantennas.

To further probe the plasmonic coupling efficiency of bowtie antenna with the nanowire, the power dependent photoluminescence characteristics under the transverse-polarized light excitation are shown in Fig. 2 (a). Besides the NBE emission at 2.26 eV (550 nm), a broad red emission of 1.72 eV (720 nm) are observed, which is ascribed to the radiative recombination from oxygen induced intermediate band (IB) states to VB.[17] A schematic of the optical transitions are shown in the band diagram (Fig. 1 (c)). For the bare nanowire, a dominant broad deep level emission at 1.6 eV with a weak NBE emission was observed under low-power excitation. It indicates the intrinsic quantum efficiency is rather low due to the presence of stacking fault defects in ZnTe/ZnTe:O/ZnO core-shell nanowire.[10,17] With increasing of the excitation power, the deep level emission transits to an IB related emission with a clear blue shift and increased intensity. The dependence of the integrated PL intensity on incident excitation power can be described by a power law fit ($I_{PL} = aP^m$), where the exponent m varies according to radiative transition channels.[28] For the bare nanowire, the exponent (m) of $\log(I) \propto \log(P)$ are 1.34 and 0.99 for the NBE and IB emissions, respectively, verifying their respective intrinsic natures of free exciton transitions and free-to-bound excitonic transitions. At high excitation condition, the intensity of IB emission is saturated and dropped due to the limited density of states of the intermediate band, while NBE emissions increase continuously in intensity.[17] In comparison, both NBE and IB emissions of the nanowire/antenna structure are enhanced, which has been normally regarded as the surface enhanced fluorescence (SEF) [29]. However, the enhancement magnitude from nanowire/antenna structure exhibits a strong dependence on excitation power. Under a low excitation power of 0.24 mW, both NBE and IB emissions of nanowire/antenna hybrid structure yield a dramatic enhancement about one order of magnitude in intensity as compared to the identical

nanowire without antenna, consistent with the polarized photoluminescence data shown in Fig. S1. As the excitation power is increased, the emission enhancement ratio of I/I_0 decreases from 11.8 (3.43) to 2.27 (1.25) for the NBE (IB) emissions (Fig. 2 (b)). The sublinear dependence of intensity on the excitation power was observed for both NBE and IB emissions with reduced exponent factors (*m*) of 0.62 and 0.25, respectively. It suggests that the magnitude of plasmonic enhanced fluorescence is not only determined by the modification of the radiative and nonradiative decay rates but also exhibits strong correlation with the intrinsic quantum yield of the nanowire emitter .[5, 30-33]

For a spectrally modified SEF, given the excitation power is far below saturation, the emission enhancement is normally determined through the expression $\frac{I}{I_0}=\frac{\gamma_{em}}{\gamma_{em}^0}=\frac{\gamma_{exc}}{\gamma_{exc}^0}\cdot\frac{\eta}{\eta^0}=\left|\frac{\mathbf{E}_{loc}}{\mathbf{E}_{loc}^0}\right|^2\cdot\frac{\eta}{\eta^0}$, where the superscript '0' is corresponding to the bare nanowire, *I* is the fluorescence intensity, and the fluorescence rate γ_{em} is the product of excitation rate γ_{exc} and quantum efficiency η.[32, 34-35] As the excitation and emission processes are not coherent, it is reasonable to treat these two processes independently.[34] Below saturation, the excitation rate (or absorption rate) is proportional to the absorption cross section or the square of near-field intensity at the excitation frequency. Thus the enhancement ratio of excitation rate is given by $\gamma_{exc}/\gamma_{exc}^0=q_{abs}/q_{abs}^0=\left|\mathbf{E}_{loc}\right|^2/\left|\mathbf{E}_{loc}^0\right|^2$, where $q_{abs}\left(q_{abs}^0\right)$ represents the absorption efficiency of nanowire with and without coupling to the antenna. [31] Fig. 3 (a) shows the absorption efficiency spectra for the nanowire with and without coupling to the bowtie antenna, calculated by three-dimensional finite-difference time-domain (3D-FDTD) simulation using a total-field-scattered-field (TFSF) source with polarization perpendicular to the nanowire axis.[32] Overall, the absorption efficiency is enhanced in the presence of antenna. In particular, the absorption peaks at 550 and 690 nm is a consequence of strong interplay of dielectric and plasmonic resonances supported by the TM_{31}/TE_{21} and TM_{21}/TE_{11} degenerated leaky resonance modes as denoted in Fig. 3 (a), which exactly match the energy levels of VB-CB and VB-IB transitions, respectively.[16] The simulated electric field distribution indicates that the dimer antennas can strongly concentrate incident

light in the nanowire by the localized surface plasmon (LSP) resonances with transverse polarization[16]. Under excitation with a transverse-polarized 514nm incident laser, the enhancement ratio of excitation rate is calculated to be $\gamma_{exc}/\gamma_{exc}^{0}=1.42$ by integrating the electric field energy $|\mathbf{E}|^2$. For longitudinal polarization, the plasmonic bowtie antenna is only weakly coupled to the nanowire as "hot spots" of field intensity induced by LSP resonances located around the side corners of bowtie antenna far away from the nanowire.

The contribution of excitation rate enhancement can be experimentally evaluated by Raman scattering spectroscopy. [36-38] Fig.3 (b) shows the Raman scattering spectra under excitation of Ar^+ laser (514nm) with transverse polarization. As the excitation photon energy is larger than the bandgap of ZnTe:O, the photon-generated excitons are efficiently coupled to the LO phonons via the long-range Frohlich interaction, leading to the profound resonance features with *n*th-order LO phonon modes dominating the spectra, while TO modes induced by deformation potential are insensitive and not observed.[29] When the nanowire/antenna structured is optically excited, an obvious increase in intensity is observed with an enhancement ratio (f_R) of 1.72 and 1.98 for 1LO and 2LO phonons, respectively. The polarized Raman spectra shown in Supplementary Information Fig. S2 indicate that the plasmonic antenna has a more profound modification on the LO phonon intensity in the case of transverse polarization. The enhanced Raman scattering feature in the vicinity of plasmonic nanostructures is typically regarded as surface enhanced Raman scattering (SERS), [39-40] in which, the Raman enhancement factor is proportional to the fourth power of local electric field $\left(|\mathbf{E}_{loc}|^4\right)$. [39-40] In this regard, given the same excitation condition, the Raman intensity enhancement factor (f_R) of nanowire/hybrid structure to the bare nanowire is proportional to $|\mathbf{E}_{loc}|^4/|\mathbf{E}_{loc}^0|^4$ or $\left(\gamma_{exc}/\gamma_{exc}^0\right)^2$. Based on the calculated absorption efficiency enhancement, a calculated Raman intensity enhancement ratio of $f_R=1.42^2=2.02$ can be yielded, which is consistent with the above experimental enhancement factors for the LO phonon peaks.

Another dominant mechanism driving the observed emission enhancement could be an increased spontaneous emission rate via the the Purcell effect [41]. To probe the contribution of spontaneous emission rate on the quantum efficiency enhancement, we performed the time-resolved photoluminescence spectroscopic (TRPL) characterization. Fig. 4 (a) shows integrated TRPL spectra of nanowire with and without antenna, respectively, under excitation of a 375 nm pulsed laser with transverse polarization. Possibly, due to different penetration depths and excitation power of incident laser, the PL spectrum is somewhat different to that in Fig.2 excited by a 514 nm Ar^+ continuous-wave laser. Nevertheless, the main features of PL emission enhancement are consistent, confirming the essential role of plasmonic coupling in enhancing the quantum efficiency of NBE and IB emissions. Fig. 4 (b) shows the TRPL spectra monitored at the NBE emission position of 550 nm, which can be reproduced by a two-component exponential function of $I(t)=A_f \exp\left(-t/\tau_f\right)+A_s \exp\left(-t/\tau_s\right)$, where $\tau_f\left(\tau_s\right)$ and $A_f\left(A_s\right)$ represent lifetime and weight factor of the fast (slow) decay processes. Both the fast decay rates $\left(1/\tau_f\right)$ and slow decay rates $\left(1/\tau_s\right)$ increase from 1/392 to 1/305 ps^{-1} and from 1/3.35 to 1/2.86 ns^{-1}, respectively. The average spontaneous decay rate $\gamma^0\left(\gamma\right)$ obtained from the relationship of $\langle\gamma\rangle=\left(1/\langle\tau\rangle\right)=\left(A_f\tau_f+A_s\tau_s\right)/\left(A_f\tau_f^{\,2}+A_s\tau_s^{\,2}\right)$ is calculated to be 0.34 and 0.39 ns^{-1}, respectively, for bare nanowire and nanowire/antenna hybrid structure. This finding strongly indicates that plasmonic coupling to the antenna contributes to the enhanced spontaneous emission decay rate and thus accelerates photon radiation by increasing the optical density of states and strengthening the plasmon-exciton coupling in the nanowire emitter via the Purcell effect. [42,43]

The potential for Purcell enhancement due to the coupling of nanowire to the strongly localized electric field inside the bowtie gap can be investigated by detailed numerical FDTD simulations. For simplicity, a harmonic dipole source with transverse polarization is placed in the antenna gap where the maximum electric field is located. We note that the pair numbers of bowtie structure and the mesoscopic size of nanowire might lead to a modified light-matter interaction in strongly confined

plasmonic fields, resulting in slight changes of calculated radiative decay rates and quantum efficiency, as shown in Supplementary Information Fig. S4. Nevertheless, this point-dipole approximation using periodic boundary conditions yields proper indications of the radiative coupling between the nanowire and plasmonic antenna. The intrinsic quantum efficiency of ZnTe:O material is defined as $\eta^0 = \gamma_r^0 / \left(\gamma_r^0 + \gamma_{nr}^0\right)$ and the modified quantum efficiency in the configuration of nanowire or hybrid nanowire/antenna structures as $\eta = \gamma_r / \gamma = \gamma_r / \left(\gamma_r + \gamma_{nr}^0 + \gamma_{nr}\right)$, where γ_r^0 and γ_{nr}^0 are the intrinsic radiative decay rate and intrinsic non-radiative decay rate, and an additional non-radiative rate γ_{nr} is accounted for the loss due to bowtie antenna absorption. As shown in Supplementary Information Fig. S3, by calculating the total optical power of a dipole source (P) and the power emitted in the far field (P_{far}), and assuming the intrinsic quantum efficiency $\eta^0 = 1$, the modified quantum efficiency in the presence of bowtie antenna can be simplified as $\eta = P_{far} / P$.[32-33] Based on this assumption, the radiative decay rates, non-radiative decay rates and the corresponding quantum efficiency in a bare nanowire and in a hybrid nanowire/antenna structure have been calculated by FDTD simulations. The radiative decay rate of the bare nanowire with an optimal diameter of 180 nm exhibits two clear resonance bands at 550 and 680 nm corresponding to TM_{31}/TE_{21} and TM_{21}/TE_{11} degenerated leaky modes, respectively (Fig.5 (a)). In the presence of the bowtie antenna, the interaction between LSPR and dielectric resonances strengthens the exciton-plasmon coupling and result in an enhancement of radiative decay rates for NBE and IB emissions, respectively, while keeping the nonradiative absorption weaker in a wide spectral range to avoid emission quenching. This is consistent with the changes of emission decay rate observed in TRPL spectra. It strongly indicates that this hybrid nanowire/antenna system is capable of sustaining multiple resonance modes that can modify the quantum efficiency by increasing the optical density of states via Purcell effect. The enhancement ratios of quantum efficiency for the spectral bands corresponding to NBE and IB emissions are calculated to be 1.15 and 1.52, respectively. Fig. 5 (b) and (c) shows the distribution of electric near-

fields with and without the metallic bowtie antenna. For the bare nanowire, the electric fields monitored at 550 nm is mostly confined within the nanowire in the form of the standing waves due to the longitudinal F-P resonance along the nanowire, while the spatial distribution of electric field monitored at 720 nm expands out of the nanowire with a standing-wave pattern surrounding the nanowire. In comparison, when the nanowire is coupled to the antenna, "hot spots" with maximum intensity of electric near-field for the wavelength of 550 nm can be observed in the nanowire close to the metal tips. The localized surface plasmons formed at the metal tips extend into the dielectric nanowires and enhance the near-field intensity within the gap of the bowtie antenna. The field enhancement within the gap is more distinguished for the spectral band centered at the wavelength of 720 nm, which matches the lower-order TM_{21}/TE_{11} degenerated leaky resonance modes. Therefore, it may interpret the larger enhancement of radiative decay rates and quantum efficiency in the long wavelength region in Fig. 5 (a) and more profoundly enhanced IB emission in Fig. 4 (a).

Taking the enhancement of excitation rates ($\gamma_{exc}/\gamma_{exc}^{0}=1.42$) and quantum efficiency into account, the product of these two calculated terms leads to small enhancement ratios of 1.63 and 2.15 for NBE and IB emissions, respectively. It is consistent with the experimental results for high-power excitation case, but cannot interpret the power-dependent enhancement features in Fig. 2. In fact, ZnTe nanostructures have a relatively low quantum efficiency of up to 60% [18-19], and therefore the intrinsic non-radiative recombination of ZnTe:O cannot be ignored. The non-radiative decay rates, normalized as $\left(\gamma_{nr}+\gamma_{nr}^{0}\right)/\gamma_{nr}^{0}$, exhibits a strong dependence on the intrinsic quantum yield of the emitter η^{0} as expressed by the relationship of $\frac{\gamma_{nr}+\gamma_{nr}^{0}}{\gamma_{nr}^{0}}=\frac{\gamma}{\gamma^{0}}\frac{\left(1-P_{far}/P\right)}{1-\eta^{0}}+\frac{P_{far}}{P}$ and the modified quantum efficiency can be rewritten as $\eta=\frac{P_{far}}{P}\cdot\frac{\gamma^{0}}{\gamma}\cdot\left(\eta^{0}+\frac{\gamma}{\gamma^{0}}-1\right)$. [31] Thus, for an emitter with high η^{0}, the margin for improvement of quantum efficiency is minimal. Conversely, when η^{0} is low, the enhancement of radiative decay rate has more profound impact on the quantum efficiency enhancement.

With this knowledge, under low excitation condition, the bare ZnTe nanowire exhibits weak emission due to rather low intrinsic quantum efficiency, i.e. $\eta^0 < 0.1$.[17] The plasmonic bowtie antennas with strong geometric resonances have more profound effect on the modification of radiative decay rates due to local field enhancement. The enhanced ratio of quantum efficiency (η/η^0) becomes large, resulting in amplified emissions about one order of magnitude (Fig.2 (b)). As excitation power increases, the non-radiative channel is saturated by increasing excess photo-excited carriers and the radiative decay becomes dominant, resulting in the increased η^0. In this case, the addition of antenna has a diminished effect on the modification of radiative and non-radiative rates as well as the quantum efficiency. As η^0 reaches 50%, only a limited enhancement in quantum efficiency can be obtained.[31] For an extreme case, as $\eta^0 \to 1$, the modified quantum efficiency coupled to nano-antenna is decreased to $\eta \to P_{far}/P < 1$. The changes of quantum efficiency is in good agreement with the experimental observation in Fig. 2. Therefore, an efficient design of plasmonic nanoatenna can significantly enhance the quantum yield of low-efficiency emitters.

In summary, distinct modification of the emission properties of ZnTe/ZnTe:O/ZnO core-shell nanowire was demonstrated by coupling it to a one-dimensional Al bowtie antenna array. The combination of enhanced near-field intensity from LSPRs and strong exciton-plasmon coupling in nanowire-antenna system gives rise to an increased excitation rate and quantum efficiency, resulting in enhanced Raman scattering and photoluminescence emissions. This work demonstrates that tailoring light-mater interaction in such nanowire-antenna hybrid system is able to yield a broadband absorption and strong light harvesting effect, which holds great promise for high performance optical devices with applications ranging from improved light sources, photovoltaics and smart sensors.

Methods.

Nanowire growth and fabrication. For nanowire growth, a 3 nm-thick Au layer was deposited on

GaSb (100) wafer by using an electron beam evaporation system (PVD75, Kurt J. Lesker Company) after removing the native oxide using dilute hydrofluoric (HF) acid. The wafer was then annealed in Ar ambient at 380 ^{0}C for 10 min to produce Au nanoparticles as the growth catalysts. ZnTe nanowires were then grown via the vapor-liquid-solid (VLS) growth mechanism at a substrate temperature of 470 ^{0}C in a horizontal quartz tube furnace by using a homemade chemical vapor transport system. The nanowires were mechanically transferred onto the SiO_2/Si substrates and controlled oxidization processes were performed at 250^{0}C in another horizontal quartz tube furnace under oxygen ambient at atmospheric pressure for four hours. Oxygen diffusion leads to the formation of a p-i-n ZnTe/ZnTe:O/ZnO heterojunction perpendicular to the growth direction. Then one-dimensional Al bowtie antenna arrays (50 nm Al in thickness) surrounding the nanowire were fabricated by electron beam lithography (Raith, EBPG5150), electron-beam evaporation (PVD75, Kurt J. Lesker Company) and liftoff. Then the core-shell nanowires were mechanically transferred onto the templates with pre-patterned Al bowtie antennas.

Characterization. The morphology was characterized by field emission scanning electron microscopy (FESEM, Zeiss) operating at 5 kV. Raman scattering and photoluminescence spectroscopy measurements were performed at room temperature using a Micro-Raman spectrometer system (Horiba JY T64000) in a backscattering configuration with a 514 nm Ar^+ laser as the excitation source. The laser was focused using a 100× objective for a spot size of ~2 μm in diameter and the excitation power was ranged from 0.02 to 2.44 mW. Time-resolved photoluminescence (TRPL) measurement was carried out at room temperature in a micro-PL system equipped with an excitation source of a 375 nm pulsed diode laser in conjunction with an Intensified Charge Coupled Device (ICCD) and a time-correlated single photon counting analyzer. The pulsed laser has a pulse width of 50 ps and an average power of 0.15 mW.

Numerical calculations. Three-dimensional FDTD simulations were performed using a commercial software package (Lumerical FDTD Solutions software). Throughout this paper, the permittivity of Al follows the Lorentz-Drude model at all operating wavelengths, and the wavelength dependent absorption coefficient, refractive index of ZnTe and ZnO materials are obtained from previous reports.[44-45] In the simulation of the absorption process, a vertically incident broadband plane-wave source with transverse polarization is used. The absorption efficiency was calculated by integrating the square of electric field amplitude of detected light with respect to that of incident light within NW. For the simulation of radiative and non-radiative decay rates, and quantum efficiencies, we set a harmonic dipole source located at the middle of the antenna gap which has a broadband emission and a polarization perpendicular to the nanowire axis. The specific dimensions of nanowire and antennas was obtained from the SEM images. Periodic boundary conditions are used to mimic more accurately the real nanowire system.

Acknowledgments

This research was supported by the National Key Research and Development Program of China (No. 2017YFB0403003), the National Natural Science Foundation of China (Nos. 61274058, 61774081, 61322403 and 11227904), the Natural Science Foundation of Jiangsu Province (Nos. BK20130013 and BK20161401), the Six Talent Peaks Project in Jiangsu Province (2014XXRJ001), the Priority Academic Program Development of Jiangsu Higher Education Institutions, the Fundamental Research Funds for the Central Universities (021014380093 and 021014380085) and the Australian Research Council. The authors also thank the partial support from Funding of Education Department of Guizhou Province, China (No. KY [2016] 326), Research Center of Optical Communications Engineering & Technology, Jiangsu Province (ZXF20170303), NUPTSF (Grant No. NY217121).

References

(1) Zhao, W.; Wang, S.; Liu, B.; Verzhbitskiy, I.; Li, S.; Giustiniano, F.; Kozawa, D.; Loh, K. P.; Matsuda, K.; Okamoto, K.; Oulton, R. F.; Eda, G. Exciton–Plasmon Coupling and Electromagnetically Induced Transparency in Monolayer Semiconductors Hybridized with Ag Nanoparticles. *Adv. Mater.* **2016**, 28, 2709-2715.

(2) Strelow, C.; Theuerholz, T. S.; Schmidtke, C.; Richter, M.; Merkl, J. P.; Kloust, H.; Ye, Z.; Weller, H.; Heinz, T. F.; Knorr, A.; Lange, H. Metal−Semiconductor Nanoparticle Hybrids Formed by Self-Organization: A Platform to Address Exciton−Plasmon Coupling. *Nano Lett.* **2016**, 16, 4811-4818.

(3) Fofang, N. T.; Grady, N. k.; Fan, Z.; Govorov, A. O.; Halas, N. J. Plexciton Dynamics: Exciton-Plasmon Coupling in a J-Aggregate-Au Nanoshell Complex Provides a Mechanism for Nonlinearity. *Nano Lett*. **2011**, 11, 1556-1560.

(4) Zhou, L.; Tan, Y.; Wang, J.; Xu, W.; Yuan, Y.; Cai, W.; Zhu, S.; Zhu, J. 3D Self-Assembly of Aluminium Nanoparticles of Plasmon-Enhanced Solar Desalination. *Nat. Photonics* **2016**, 10, 393-398.

(5) Kinkhabwala, A.; Yu, Z.; Fan, S.; Avlasevich, Y.; Mullen, K.; Moerner, W. E. Large Single-Molecule Fluorescence Enhancements Produced by a Bowtie Nanoantenna. *Nat. Photonics* **2009**, 3, 654-657.

(6) Brongersma, M. L.; Halas, N. J.; Nordlander, P. Plasmon-Induced Hot Carrier Science and Technology. *Nat. Nanotechnol.* **2015**, 10, 25-34.

(7) Clavero, C. Plasmon-Induced Hot-Electron Generation at Nanoparticle/Metal-Oxide Interfaces for Photovoltaic and Photocatalytic Devices. *Nat. Photonics* **2014**, 8, 95-103.

(8) Sobhani, A.; Knight, M. W.; Wang, Y. M.; Zheng, B.; King, N. S.; Brown, L. V.; Fang, Z. Y.; Nordlander, P.; Halas, N. J. Narrowband Photodetection in the Near-Infrared with a Plasmon-Induced Hot Electron Device. *Nat. Commun.* **2013**, 4, 1643.

(9) Sun, D.; Aivazian, G.; Jones, A. M.; Ross, J. S.; Yao, W.; Cobden, D.; Xu, X. D. Ultrafast Hot-

Carrier-Dominated Photocurrent in Graphene. *Nat. Nanotechnol.* **2012**, 7, 114-118.

(10) Zhang, Q.; Liu, X.; Utama, M. I. B.; Zhang, J.; de la Mata, M.; Arbiol, J.; Lu, Y.; Sum, T. C.; Xiong, Q. H. Highly Enhanced Exciton Recombination Rate by Strong Electron− Phonon Coupling in Single ZnTe Nanobelt. *Nano Lett.* **2012**, 12, 6420-6427.

(11) Wang, W.; Lin, A. S.; Phillips, J. D.; Metzger, W. K. Generation and Recombination Rates at ZnTe:O Intermediate Band States. *Appl. Phys. Lett.* **2009**, 95, 261107.

(12) Tanaka, T.; Kume, Y.; Nishio, M.; Guo, Q.; Ogawa H.; Yoshida, A. Fabrication of ZnTe Light-Emitting Diodes Using Bridgman-Grown Substrates. *Jpn. J. Appl. Phys.* **2003**, 42, L362-L364.

(13) Luque, A.; Marti, A.; Stanley, C. Understanding Intermediate-Band Solar Cells. *Nat. Photonics* **2012**, 6, 146-152.

(14) Jang, Y. J.; Lee, J.; Lee, J.; Lee, J. S. Solar Hydrogen Production from Zinc Telluride Photocathode Modified with Carbon and Molybdenum Sulfide. *ACS Appl. Mater. Interfaces*, **2016**, 8, 7748-7755.

(15) Kang, Z. T.; Summers, C. J. ZnTe:O Phosphor Development for X-Ray Imaging Applications. *Appl. Phys. Lett.* **2006**, 88, 111904.

(16) Nie, K. Y.; Li, J.; Chen, X.; Xu, Y.; Tu, X.; Ren, F. F.; Du, Q. G.; Fu, L.; Kang, L.; Tang, K.; Gu, S.; Zhang, R.; Wu, P.; Zheng, Y.; Tan, H. H.; Jagadish, C.; Ye, J. D. Extreme Absorption Enhancement in ZnTe:O/ZnO Intermediate Band Core-Shell Nanowires by Interplay of Dielectric Resonance and Plasmonic Bowtie Nanoantennas *Sci. Rep.* **2017**, 7, 7503.

(17) Choi, S. B.; Song, M. S.; Kim, Y. O-Doping Profile along ZnTe Nanowires Obtained Using Power Dependent Microphotoluminescence Measurements. *J. Phys. Chem. C* **2016**,120, 24457-24462.

(18) Hou, L.; Zhang, Q.; Ling, L.; Li, C. X.; Chen, L.; Chen, S. Interfacial Fabrication of Single-Crystalline ZnTe Nanorods with High Blue Fluorescence. *J. Am. Chem. Soc*. **2013**, 135, 10618-10621

(19) A. F. Bu, H. B.; Kim, D. Quick Synthesis of Water-soluble, Luminescent ZnTe Nanoparticles by Hydrothermal Technique. *Chem. Lett*. **2018**, 47, 152-155

(20) Lee, B.; Park, J.; Han, G. H.; Ee, H. S.; Naylor, C. H.; Liu, W.; Johnson, A. T. C.; Agarwal, R.

Fano Resonance and Spectrally Modified Photoluminescence Enhancement in Monolayer MoS2 Integrated with Plasmonic Nanoantenna Array. *Nano Lett.* **2015**, 15, 3646-3653.

(21) Dong, L.; Yang, X.; Zhang, C.; Cerjan, B.; Zhou, L.; Tseng, M. L.; Zhang, Y.; Alabastri, A.; Nordlander, P.; Halas, N. J. Nanogapped Au Antennas for Ultrasensitive Surface-Enhanced Infrared Absorption Spectroscopy. *Nano Lett.* **2017**, 17, 5768-5774.

(22) Eggleston, M. S.; Messer, K.; Zhang, L.; Yablonovitch, E.; Wu, M. C. Optical Antenna Enhanced Spontaneous Emission. *PNAS* **2015**,112, 1704-1709.

(23) Casadei, A.; Llado, E.A.; Amaduzzi, F.; Russo-Averchi, E.; Ruffer, D.; Heiss, M.; Negro, L.D.; I Morral, A. F. Polarization response of nanowires a` la Carte. *Sci. Rep*. **2015**, 5, 7651

(24) Rodriguez, S. R. K.; Abass, A.; Maes, B.; Janssen, O. T. A.; Vecchi, G.; Rivas G. J. Coupling Bright and Dark Plasmonic Lattice Resonances. *J. Phys. Rev. X* **2011**, 1, 021019.

(25) Giannini, V.; Fernandez-Dominguez, A. I.; Heck, S. C.; Maier, S. A. Plasmonic Nanoantennas: Fundamentals and Their Use in Controlling the Radiative Properties of Nanoemitters. *Chem. Rev.* **2011**,111, 3888-3912.

(26) Fromm, D. P.; Sundaramurthy, A.; James Schuck, P.; Kino, G.; Moerner, W. E. Gap-Dependent Optical Coupling of Single "Bowtie" Nanoantennas Resonant in the Visible. *Nano Lett.* **2004**, 4, 957-961.

(27) Wang, J.; Gudiksen, M. S.; Duan, X.; Cui, Y.; Lieber, C. M. Highly polarized photoluminescence and photodetection from single indium phosphide nanowires. *Science* 2001, 293, 1455-1457

(28) Schmidt, T.; Lischka, K.; Zulehner, W. Excitation-Power Dependence of The Near-Band-Edge Photoluminescence of Semiconductors. *Phys. Rev. B* **1992**, 45, 8989-8994.

(29) Li, Z.; Li, Y.; Han, T.; Wang, X.; Yu, Y.; Tay, B.; Liu, Z.; Fang, Z. Tailoring MoS_2 Exciton−Plasmon Interaction by Optical Spin−Orbit Coupling. *ACS Nano* **2017**, 11, 1165-1171.

(30) Sun, G.; Khurgin, J. B.; Soref, R. A. Practical Enhancement of Photoluminescence by Metal Nanoparticles. *Appl. Phys. Lett.* **2009**, 94, 101103.

(31) Giannini, V.; Sanchez-Gil, J. A.; Muskens, O. L.; Rivas, J. G. Electrodynamic calculations of spontaneous emission coupled to metal nanostructures of arbitrary shape: nanoantenna-enhanced fluorescence. *J. Opt. Soc. Am. B* **2009**, 26, 1569-1577

(32) Meng, X.; Grote, R. R.; Dadap, J. I.; Panoiu, N. C.; Osgood, Jr. R. M. Engineering metal-nanoantennae/dye complexes for maximum fluorescence enhancement. *Opt. Express*, **2014**, 22, 22018-22030

(33) Bharadwaj, P.; Novotny, L. Spectral dependence of single molecule fluorescence enhancement, *Opt. Express* **2007**, 15, 14266-14274

(34) Chowdhury, M. H.; Pond, J.; Gray S. K.; Lakowicz, J. R. Systematic Computational Study of the Effect of Silver Nanoparticle Dimers on the Coupled Emission from Nearby Fluorophores. *J. Phys. Chem. C* **2008**, 112, 11236-11249.

(35) Kuhn, S.; Hakanson, U.; Rogobete, L.; Sandoghdar, V. Enhancement of Single-Molecule Fluorescence Using a Gold Nanoparticle as an Optical Nanoantenna. *Phys. Rev. Lett.* **2006**, 97, 017402.

(36) Zhang, Q.; Zhang, J.; Utama, M. I. B.; Peng, B.; de la Mata, M.; Arbiol, J.; Xiong, Q. H. Exciton-Phonon Coupling in Individual ZnTe Nanorods Studied by Resonant Raman Spectroscopy. *Phys. Rev. B* **2012**, 85, 085418.

(37) Ketterer, B.; Heiss, M.; Uccelli, E.; Arbiol, J.; Morra, A. F. I. Untangling the Electronic Band Structure of Wurtzite GaAs Nanowires by Resonant Raman Spectroscopy. *ACS Nano* **2011**, 5, 7585-7592.

(38) Amaduzzi, F.; Llado, E. A.; Hautmann, H.; Tanta, R.; Matteini, F.; Tutuncuoglu, G.; Vosch, T.; Nygard, J.; Jespersen, T.; Uccelli, E.; I Morral, A. F. Tuning the response of non-allowed Raman modes in GaAs nanowires. *J. Phys. D: Appl. Phys*. **2016**, 49, 095103

(39) Koch, R. J.; Fryska, S.; Ostler, M.; Endlich, M.; Speck, F.; Hansel, T.; Schaefer, J. A.; Seyller, T. Robust Phonon-Plasmon Coupling in Quasifreestanding Graphene on Silicon Carbide. *Phys. Rev. Lett.* **2016**, 116,106802.

(40) Jorio, A.; Mueller, N. S.; Reich, S. Symmetry-Derived Selection Rules for Plasmon-Enhanced Raman Scattering. *Phys. Rev. B* **2017**, 95, 155409.

(41) Zhang, G.; Zhuang, Z.; Guo, X.; Ren, F. F.; Liu, B.; Ge, H.; Xie, Z.; Sun, L.; Zhi, T.; Tao, T.; Li, Y.; Zheng, Y.; Zhang, R. Bloch Surface Plasmon Enhanced Blue Emission from InGaN/GaN Light-Emitting Diode Structures with Al-Coated GaN Nanorods. *Nanotechnology*, **2015**, 26, 125201.

(42) Luo, Y.; Ahmadi, E. D.; Shayan, K.; Ma, Y.; Mistry, K. S.; Zhang, C.; Hone, J.; Blackburn J. L.; Strauf, S. Near-Unity Quantum Yield From Carbon Nanotube Excitons Coupled to Plasmonic Nanocavities. *Nat. Commun.* **2017**, 8, 1413.

(43) Mauser N.; Hartschuh, A. Tip-Enhanced Near-Field Optical Microscopy. *Chem. Soc. Rev.* **2014**, 43, 1248-1262.

(44) Sato, K.; Adachi, S. Optical properties of ZnTe. *J. Appl. Phys.* **1993**, 73**,** 926–931.

(45) Yoshikawa, H.; Adachi, S. Optical constants of ZnO. *Jpn J. Appl. Phys.* **1997**, 36**,** 6237-6243.

Figures and Captions

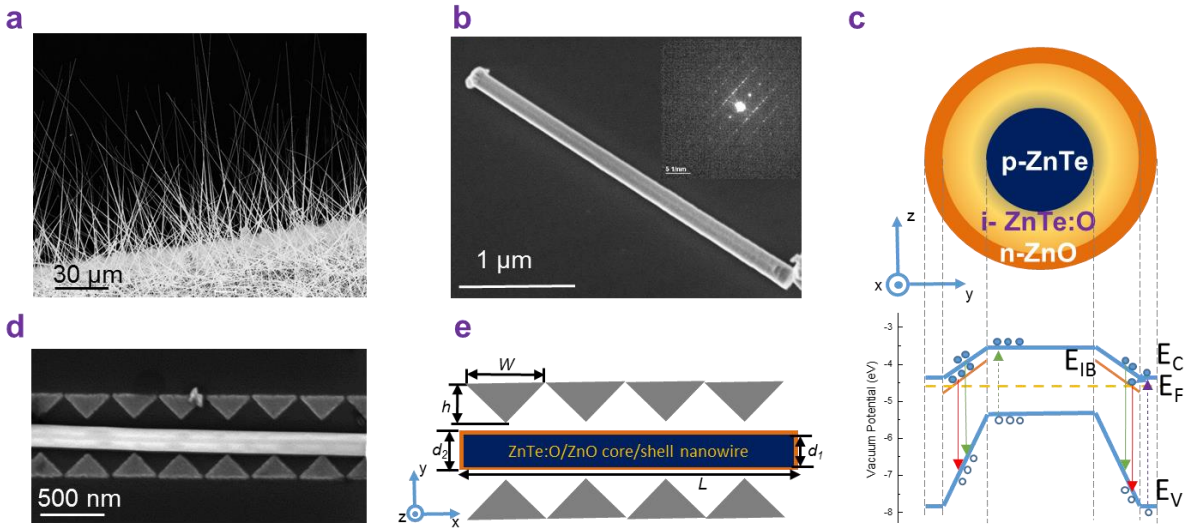

Figure 1. (a) SEM image of as-grown ZnTe nanowires on a GaSb (100) substrate; (b) single ZnTe/ZnTe:O/ZnO core-shell nanowire transferred on a Si substrate and the inset showing the SAED from TEM measurement; (c) cross-sectional schematic of the core-shell nanowire and its corresponding bandgap diagram with possible absorption and recombination transitions; (d) SEM image of a 180-nm-diameter ZnTe/ZnTe:O/ZnO core-shell nanowire located within an Al bowtie antenna array fabricated by EBL and metal lift-off processes; (e) Top-view schematic of the nanowire located within an Al bowtie antenna array depicting the various dimensions.

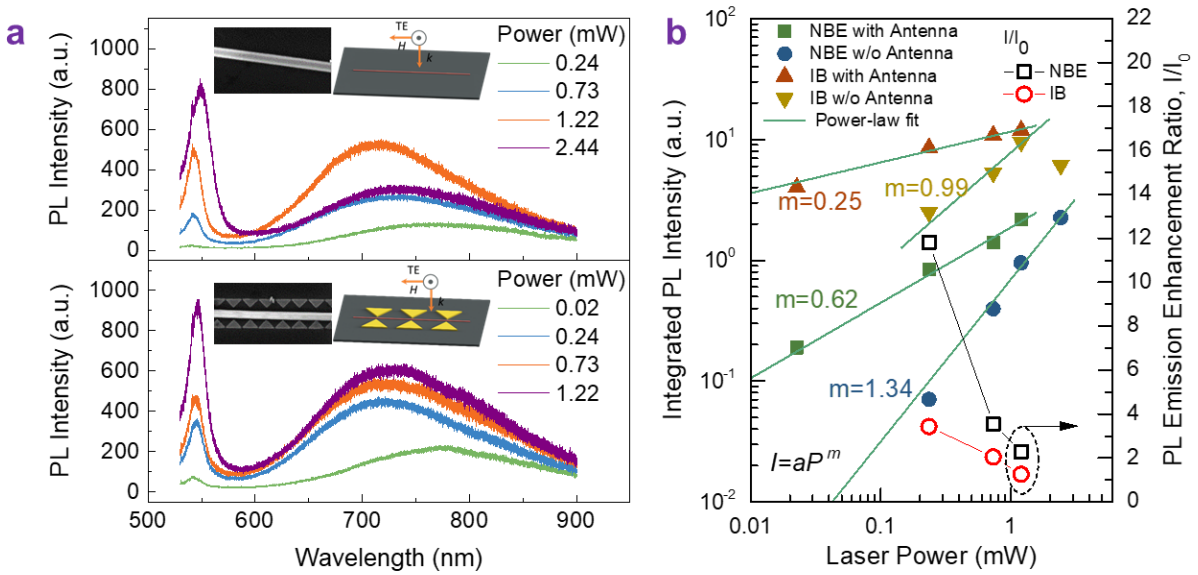

Figure 2. (a) Micro-PL from a bare nanowire and nanowire-antennas system with different excitation powers, the inserts are the SEM iamges of a nanowire with and without Al bowtie antenna array; (b) Integrated PL intensity and the corresponding Purcell enhancement factor as a function of incident laser power density.

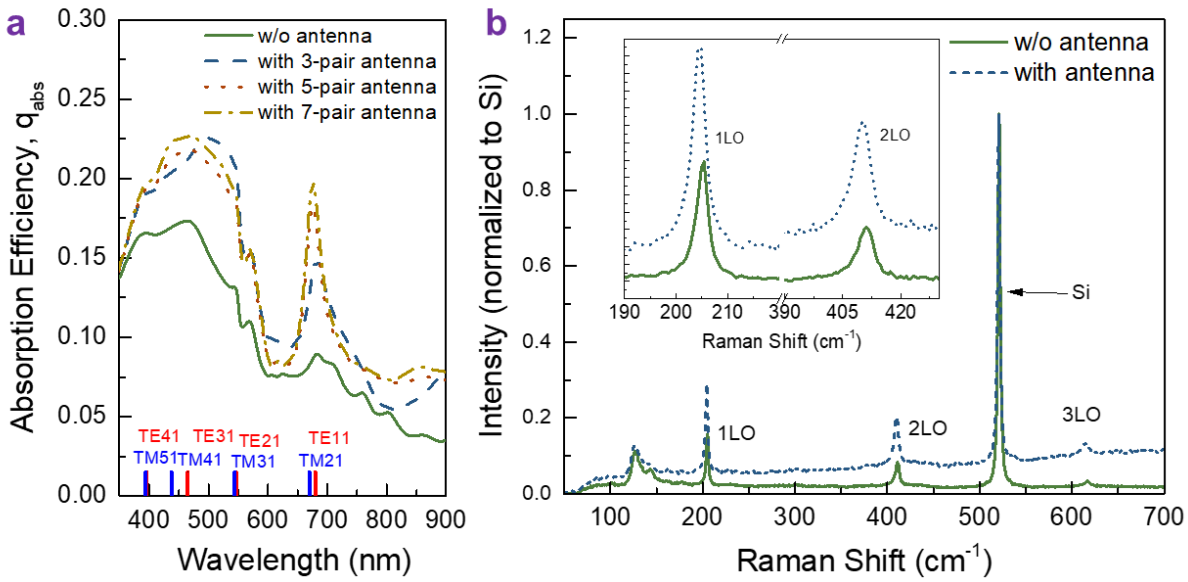

Figure 3. (a) The absorption efficiency spectra of ZnTe/ZnTe:O/ZnO core-shell nanowire without antenna and with different paired antenna calculated by FDTD using normal incident light with transverse polarization and (b) Resonance Raman scattering spectra from the bare nanowire and nanowire-antenna system.

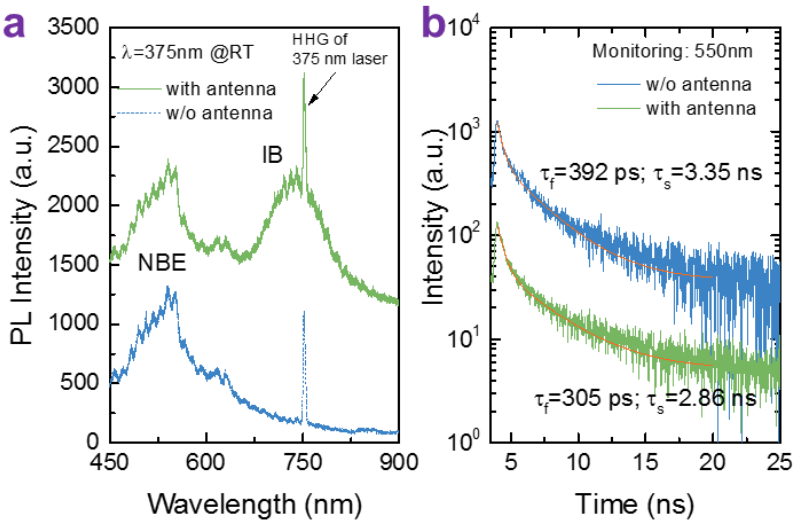

Figure 4. (a) TRPL spectra and (b) TRPL decay curves of the nanowire with and without Al bowtie antenna array under the same pump power at room temperature. In (a), the sharp peaks at 750 nm correspond to the half-harmonic generation (HHG) of the 375 nm excitation laser.

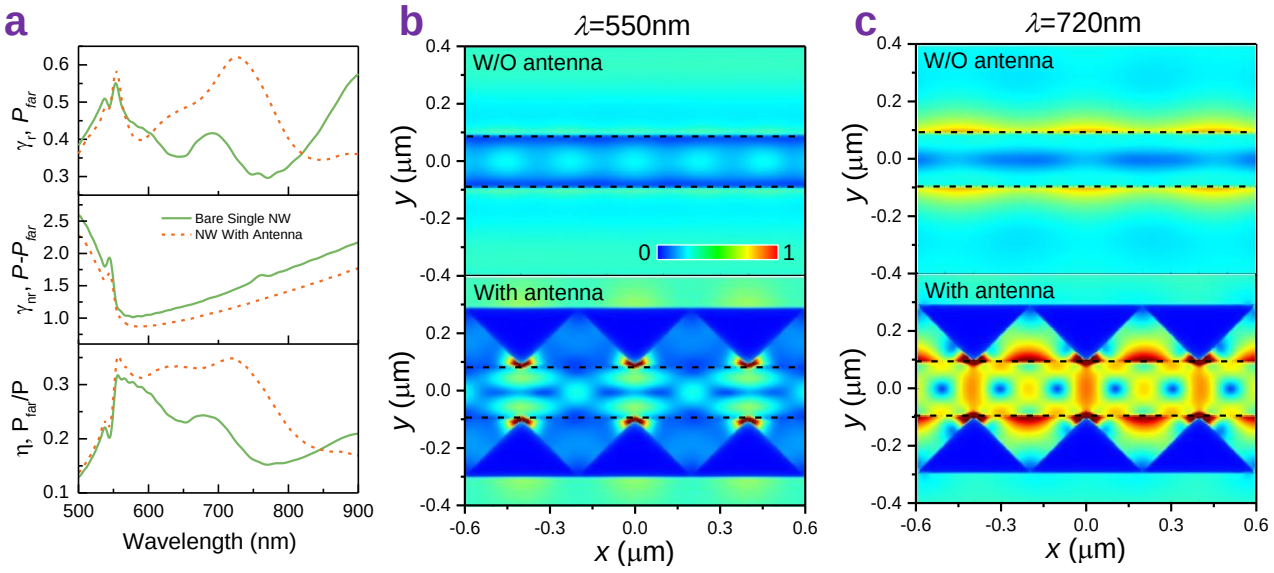

Figure 5. (a) The calculated radiative decay rates, non-radiative decay rates and quantum efficiency of ZnTe:O/ZnO nanowires with and without the coupled Al bowtie antennas. (b) Electric near-field intensity distribution in ZnTe:O/ZnO nanowire with and without the coupled Al bowtie antennas at the wavelength of (b) 550nm and (c) 720nm, which corresponding to the NBE and IB emissions.